Fingertip Position and Force Control for Dexterous Manipulation through Model-Based Control of Hand-Exoskeleton-Environment

Paria Esmatloo[1] and Ashish D. Deshpande[2]

***Abstract*— Despite mechanical advancements in assistive hand exoskeletons, the manipulation ability they provide has remained far inferior to that of a healthy human hand. State-of-the-art control strategies are mainly focused on robot joint-level position control, although accurate control of fingertip positions and forces is required for human-like dexterity. Due to nonlinear relationships between inputs and outputs, dexterous manipulation requires accurate models of interaction between the fingers, the exoskeleton, and the fingertip space. In this research, we utilize model-based control to achieve desired fingertip position and forces with a multi-degree-of-freedom (multi-DOF) exoskeleton for the first time. We compare it with conventional control methods and demonstrate the performance to be superior and within human accuracy levels.**

I. Introduction

Disability in the upper extremities has affected 20 million individuals in the United States [1]. 45% of Spinal Cord injury (SCI) patients for instance, have difficulties in daily tasks due to insufficient hand function. Human dexterity and hand function are a result of combining various capabilities like independent finger movement, reaction speed, strength, coordination, and precise control of task-specific fingertip forces [2]. Assistive devices have been developed to help affected people regain partial independence. Although the human hand is a very complex system with 27 DOF, earlier devices focused only on coupled motion of the fingers [3], [4], restraining fingers to pinching or cylindrical grasping.

Later, multi-DOF devices were developed to allow a wider range of natural grasps [5], [6], [7], [8]. Small size of the finger phalanges and limited space make it often impossible to apply direct matching between the robot and the finger joints. Thus, many exoskeletons have used linkages on the back of the hand to actuate the finger joints [9], [8], [10], [11]. In these devices, the relationships between exoskeleton angles and the finger joint angles are usually nonlinear. Most of these exoskeletons have only focused on whole-hand movements and improving strength using the simplest forms of control strategies such as robotic position control [4] or coupled movement of finger joints [12], [13], disregarding other prominent aspects of dexterity like independent finger movement, coordination, and precise control of fingertip forces. Although these approaches help with some specific needs, they ignore and even limit the various capabilities of humans in object interactions. In [14], [6], the use of a few predefined grasping poses limited SCI subjects' ability to grasp small objects and perform which require precise finger movements. In addition, previously, mainly feed-forward position control of the exoskeleton joints has been explored causing the fingers to follow a vague trajectory determined by the exoskeleton and finger interactions [9], [6], [15], [16]. Consequently, power grasping with imprecise movements of fingers has been considered as opposed to precision grasps and manipulation requiring fine control of fingertip positions and forces.

Achieving position and force control at the fingertips requires accurate models of the human hand, assistive device mechanisms, power transmission system, environment, and the interactions between them, in addition to an exoskeleton design that can actuate individual DOF of the fingers. Many researchers have studied modeling the multifaceted structure of the human hand as mechanical structures [17], [18], and the couplings between finger and joint movements to reduce the number of DOF of the hand in free motion or in a few grasp categories [19], [20]. Although these relationships can describe the finger motions in specific conditions, they generally do not hold during object interactions and force exertion at the fingertips [21]. Thus, appropriate models of the fingers should be used to fulfill the requirements of manipulation tasks.

Kinematic modeling of the exoskeleton has been considered mainly for the design and range of motion analysis [10], [8], [22], and rarely for the real-time control of precise movements of the fingers or interaction forces [23], [24]. Authors in [9], [7] developed kinematic models for the exoskeleton and the fingers. However, they only empirically validated position control at the exoskeleton joint level and did not consider controlling the finger angles or fingertip position. In [8], authors used kinematic and dynamic models of the exoskeleton to compensate for robot hindrance in virtual reality applications but only validated it in the exoskeleton joint level.

Another source of non-linearity and uncertainty in the exoskeleton control comes from power transmission mechanisms such as cable driven actuation [25], [26], [27], [9], or flexible shaft transmission [7] with remotely located actuators. Despite limited research on the accuracy of precision movements at the finger level, results indicate losses in the power transmission significantly affect the tracking results even for exoskeleton angles [8], [10], [7]. In [28], authors characterized the backlash property in Bowden cable transmission and proposed a model for feed forward torque

[1]Paria Esmatloo is a PhD student of Mechanical Engineering, The University of Texas at Austin, USA p.esmatloo@utexas.edu

[2]Ashish Deshpande is a faculty of Mechanical Engineering, The University of Texas at Austin, USA ashish@austin.utexas.edu

TABLE I: Human index (middle) finger joint limits

Joint	Minimum	Maximum
MCP	30° extension	90° flexion
	35° abduction	35° adduction
PIP	0° extension	110° flexion
DIP	0° extension	70° flexion

control at the fingers by compensating for backlash.

In this research, we take an important step towards realizing human-like grasping and manipulation through assistive hand exoskeletons by accomplishing the following objectives: 1) Provide kinematic and kinetic models for human fingers and finger-exoskeleton interaction for a fully actuated finger exoskeleton design, and a model for compensating slack in the power transmission inspired by [28]. 2) Validate the models in simulation for an everyday drawing task. 3) Demonstrate experimental results for fingertip position and force tracking through model-based control with a 2-DOF finger exoskeleton and a passive instrumented finger within human finger accuracy [29]. Finally, we discuss the implications of this methodology in wider control applications and various fields.

II. Modeling

In this section, we detail the methodology for modeling the subsystems. We assume the precision tasks are performed at low velocities, masses are relatively small, dynamic effects are negligible, and attachments between the exoskeleton and the fingers are rigid. Finger joints are modeled as friction-less revolute joints with no parallel stiffness.

A. Human Finger Model

We introduce a hierarchical linkage structure based on the human finger anatomy similar to [18] and define the joint limits in Table I [30]. There are four DOF in the index finger, namely, MCP abduction-adduction (ab-ad), MCP flexion-extension (f-e), PIP f-e, DIP f-e. We assume the two axes at the MCP joint are intersecting and perpendicular, and the PIP and DIP axes are perpendicular to the bones attached to them.

1) Kinematic Model: We utilize the modified Denavit-Hartenberg method [31] to describe the position of the fingertip as a function of the joint angles.

$$P_{f_t} = \begin{bmatrix} X_{f_t} & Y_{f_t} & Z_{f_t} \end{bmatrix}^T = f(\theta_{f,abad}, \theta_{f,mcp}, \theta_{f,pip}, \theta_{f,dip}) \quad (1)$$

2) Kinetic Analysis: The finger Jacobian is calculated by symbolically differentiating the endpoint coordinates with respect to the joint variables (Equation 2). Fingertip force is found based on joint torques in Equation 3.

$$[J_{finger}]_{3\times 4} = \frac{\partial P_{f_t}}{\partial \Theta_f} \quad (2)$$

$$\begin{bmatrix} F_f \end{bmatrix}_{3\times 1} = \begin{bmatrix} F_{f,x} \\ F_{f,y} \\ F_{f,z} \end{bmatrix} = (J_{finger}^T)^{\dagger} \begin{bmatrix} T_f \end{bmatrix}_{4\times 1} \quad (3)$$

The left pseudo inverse, $(J_{finger}^T)^{\dagger}$, is used since J_{finger} is not a square matrix.

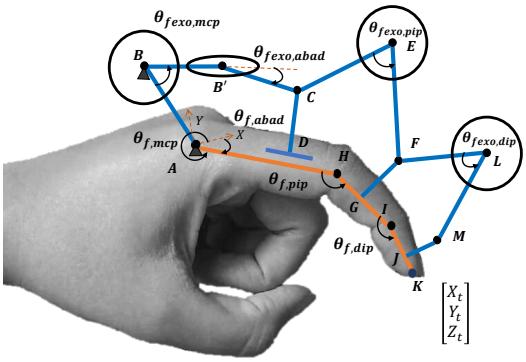

Fig. 1: Index exoskeleton mechanism

3) Inverse Kinematics: Since there are four finger joint angles and three fingertip coordinates to control, this problem is redundant, and there are infinite solutions for the joint angles. We have chosen to control the absolute flexion angle of the distal phalanx ($\theta_{f,total} = \theta_{f,mcp} + \theta_{f,pip} + \theta_{f,dip}$) as a measure of the orientation of the fingertip, besides the fingertip position.

B. Hand Exoskeleton and Finger Interaction Model

The exoskeleton design implemented is inspired by the Maestro Hand Exoskeleton [9], [32]. Maestro exoskeleton only has two actuated joints in the index finger module (f-e at the MCP and PIP). However, for fine manipulation, it is important to fully control the finger configuration. Thus, in this section, we assume a general design with all four DOF actuated.

1) Linkage Structure: Actuation of the four joints is done through three closed loop chains (Fig. 1). A slider-crank mechanism actuates f-e and ab-ad angles at the MCP joint. Unlike the finger MCP joint which has co-located axes, the exoskeleton MCP joint has a proximal f-e joint followed by the ab-ad joint. can be simplified to a planar four-bar mechanism, where the exoskeleton PIP angle controls the finger PIP angle. Similarly, finger DIP angle is controlled through a four-bar mechanism.

2) Kinematic Model: The points A and B are grounded from the hand and the exoskeleton side. We assume the points A, B, C, and D are always co-planar, and at each ab-ad angle of the exoskeleton, the mechanism ABCD is an inverted planar crank-slider mechanism. The equivalent length l_{BC} is a function of the exoskeleton ab-ad angle through the law of cosines. The closed form solution of the inverted crank slider mechanism [33] gives two equations for $\theta_{f,mcp}$ and l_{AD}, which are also coupled with the third unknown $\theta_{f,abad}$. The co-planarity condition ABCD results in Equation (4). Solving the three equations, the finger MCP angles are found based on the exoskeleton angles.

$$\theta_{f,abad} = arcsin\left(\frac{l_{B'C} sin(\theta_{fexo,abad}) cos(\theta_{fexo,mcp,abs})}{l_{AD} cos(\theta_{f,mcp})}\right) \quad (4)$$

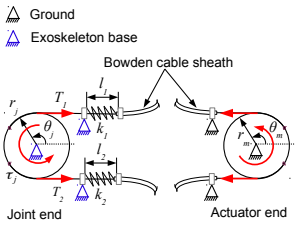

(a) Series Elastic Actuation (SEA) used in exoskeleton [9]

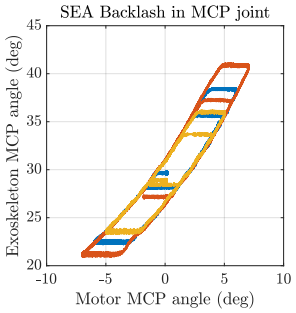

(b) Bowden cable backlash effect shown in robot MCP joint

Fig. 2: Series Elastic Actuation (SEA)

In the CEFH chain, using the solution for the kinematics of the four-bar mechanism [33], $\theta_{f,pip}$ is calculated as a function of the exoskeleton PIP angle, $\theta_{fexo,pip}$. Similarly, the kinematics of the DIP chain gives $\theta_{f,dip}$, and all the unknown finger joint angles are found as functions of the exoskeleton angles.

3) Kinetic Relationships: The Jacobian of the finger-exoskeleton system is found by partial differentiation of the finger angles with respect to the exoskeleton angles (Equation 5) using symbolic operations in MATLAB and the `Jacobian` function. The resulting finger torques are calculated based on the applied exoskeleton torques (Equation 6).

$$[J_{fexo}]_{4\times4} = \frac{\partial[\Theta_f]}{\partial[\Theta_{fexo}]} \tag{5}$$

$$[T_f]_{4\times1} = (J^T_{fexo})^{-1}[T_{fexo}]_{4\times1} \tag{6}$$

where $(J^T_{fexo})^{-1}$ is the inverse of J^T_{fexo}.

4) Inverse Kinematics: ABCD is treated as a crank-slider mechanism. The unknown angles and slider length are found from the loop equations [33]. Inverse kinematic solution for the PIP and DIP chains are found from four-bar loop equations.

C. Series Elastic Actuation Model

In the Series Elastic Actuation (SEA) design, one pulley is attached to the motor side, and another is attached to the exoskeleton joint (Fig. 2a). Power is transmitted through Bowden cables, allowing remote positioning of the actuators with respect to the hand. If we assume that the effects of friction, dynamics, and slack are negligible, the displacement of the Bowden cable on both sides would be equal and the motor angle would be $\theta_m = \frac{r_j}{r_m}(\theta_{j,d} - \theta_{j0})$, where $\theta_{j,d}$ is the desired exoskeleton joint angle. Two linear springs transmit torques on each exoskeleton joint through Equation 7, assuming no loss in the Bowden cable mechanism.

$$\tau_j = (T_2 - T_1)r_j = 2k(r_m\theta_m - r_j(\theta_j - \theta_{j0}))r_j \tag{7}$$

where T_1 and T_2 are cable tension forces, r_j and r_m are the joint and motor pulley radii, and $(\theta_j - \theta_{j0})$ is the displacement of the exoskeleton joint with respect to the resting angle.

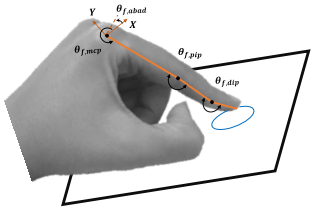

(a) Configuration of the index finger on a touchscreen

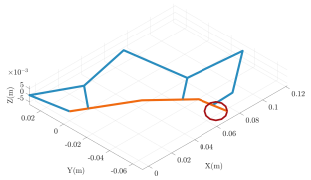

(b) Simulated circle trajectory tracking using the index fingertip

Fig. 3: Drawing a circle on a touchscreen

However, the transmission accuracy is dependent on the cable pre-tension and bending in the cable routing. In practice, Bowden cables demonstrate a behavior similar to fatigue due to slack (Fig. 2b). In [28], a model is proposed for Bowden cable slack (backlash) behavior (Equation 8).

$$\theta_j(t) = BL(\theta_m(t)) = \tag{8}$$
$$\begin{cases} \alpha(\theta_m(t) - c_r), & \dot{\theta}_m(t) > 0 \;\&\; \theta_j(t^-) = \alpha(\theta_m(t^-) - c_r) \\ \alpha(\theta_m(t) - c_l), & \dot{\theta}_m(t) < 0 \;\&\; \theta_j(t^-) = \alpha(\theta_m(t^-) - c_l) \end{cases}$$

where $\alpha = r_m/r_j$ and c_r, c_l are the right and left offsets of the backlash curve, obtained empirically. To compensate for this effect, a smooth backlash inverse model (Equation 9) is proposed [28], which determines the motor position commands to achieve a desired exoskeleton angle.

$$\begin{aligned} \theta_{m,d}(t) &= SBL^{-1}(\theta_{j,d}(t)) = \theta_{j,d}/\alpha + c_r\gamma + c_l(1-\gamma) \\ \gamma(\dot{\theta}_{j,d}(t)) &= \frac{1}{1+exp(-\rho\dot{\theta}_{j,d}(t))} \end{aligned} \tag{9}$$

where γ is a sigmoid function and ρ is a positive constant determining the degree of smoothness. The larger the ρ, the sharper the changes in the commanded motor angles to compensate for the slack.

III. Simulation

We validate the developed kinematic and kinetic models through simulation of an everyday scenario of drawing a circle using the fingertip while maintaining constant contact force.

A. Position Tracking

We consider following a circle with a diameter of 1.4 cm on a touchscreen (Fig. 3a). The plane of the screen is estimated to make a 45° angle with the XZ plane of the finger. The trajectory of the fingertip in the frame attached to the metacarpal bone is calculated and plotted in Fig. 4. Next, joint angles are found using the inverse kinematics. To resolve the redundancy, we chose the orientation of the last phalanx, with respect to the metacarpal bone, to be constant throughout the task. We defined a cost function containing the errors in the fingertip position and orientation for when an exact solution is not possible (Equation 10).

$$Cost_f = w_{x_f}\Delta X^2_{t_f} + w_{y_f}\Delta Y^2_{t_f} + w_{z_f}\Delta Z^2_{t_f} + w_{\phi_f}\Delta\phi^2_f \tag{10}$$

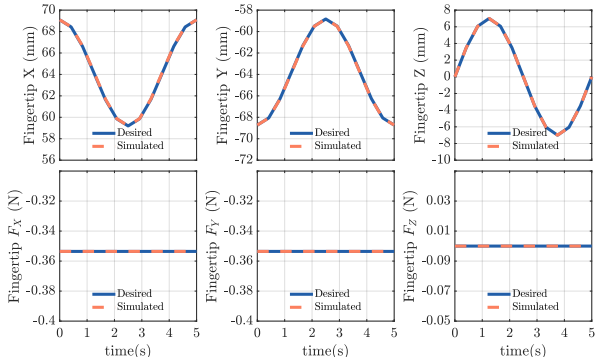

Fig. 4: Desired (solid) and simulated position of the fingertip for tracking a circle trajectory

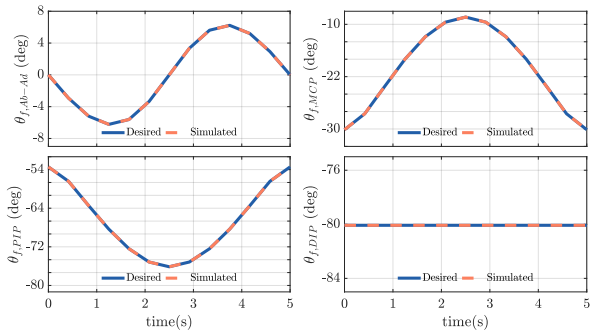

Fig. 5: Finger joint angles for circle trajectory tracking task, as calculated from inverse kinematics (solid) and forward kinematics simulation

where ΔX_{t_f}, ΔY_{t_f}, and ΔZ_{t_f} are the errors in X, Y, Z coordinates, and $\Delta\phi_f$ is the error in the orientation of the distal phalanx. w_{x_f}, w_{y_f}, w_{z_f}, and w_{ϕ_f} are the corresponding weight values, which can be altered based on the importance of the accuracies in a task. The required finger joint angles and exoskeleton angles are shown in Figs. 5 and 6.

To validate the accuracy of the complete kinematic model, we fed the calculated exoskeleton angles to the forward kinematics models. The resulting finger angles and the fingertip trajectories are shown in Fig. 5 and 4 in dotted lines and overlap with the desired values in both figures. Note the difference in the trends and relationships between

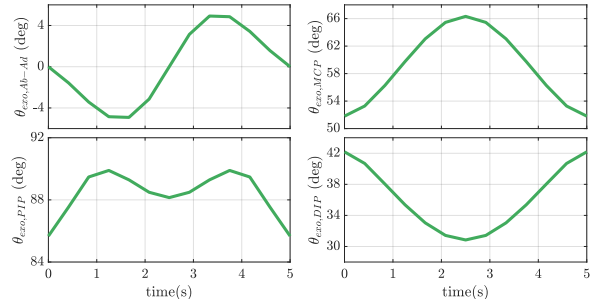

Fig. 6: Index exoskeleton joint angles for circle trajectory tracking task, as calculated from inverse kinematics

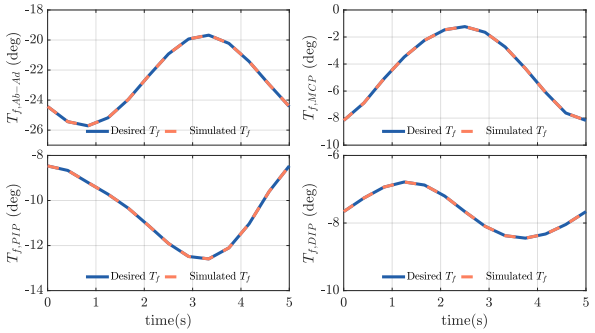

Fig. 7: Desired and simulated torques at the finger joints for drawing a circle on a touchscreen

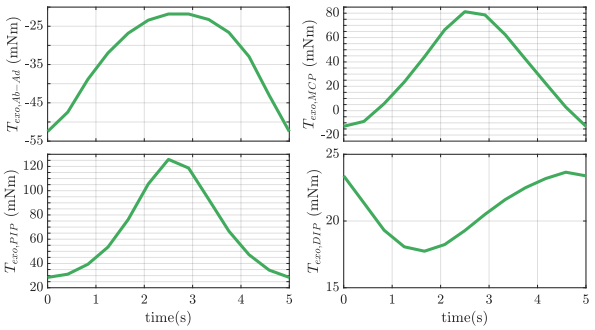

Fig. 8: Required torques at the exoskeleton joints for drawing a circle on a touchscreen

the corresponding angle and torque values in the exoskeleton and the finger joints, accentuating the necessity of interaction models in accurate fingertip level control.

B. Fingertip Force Tracking

Based on observation, desired fingertip force for touchscreen interaction is approximately 0.5 N normal to the plane. The torques required at the finger and exoskeleton joints are shown in Fig. 7 and 8. These values are fed to the forward kinematics models to find the resulting torques at the finger joints and the simulated force at the fingertip (Fig. 7 and 4).

IV. Experimental Characterization

In this section, we utilize a 2-DOF finger exoskeleton and an instrumented finger to implement the developed models in the control of exoskeleton and finger movements and forces.

A. Experiment Setup

For position tracking, the setup consists of the Maestro index exoskeleton, a 2-DOF instrumented finger, and motion capture markers (Fig. 10). Force tracking setup includes a force sensor grounded on a mechanical breadboard as well.

1) Exoskeleton Overview: The Maestro Hand Exoskeleton [6], [9], [34] consists of three finger modules for index and middle fingers, and thumb (Figure 9). There are two actuated DOF in the index and middle fingers for actuating MCP f-e and PIP f-e [9]. The thumb module has four actuated DOF. We will focus on the index module, since

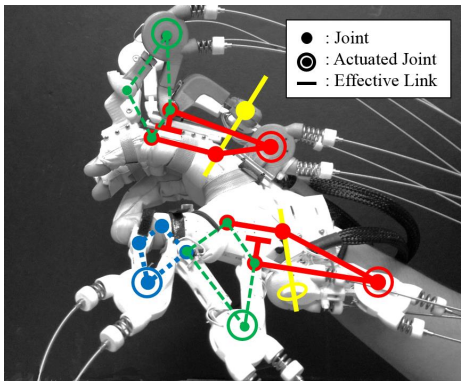

Fig. 9: Maestro exoskeleton has three actuated fingers and 8 DOF. The actuation of the joints are done through slider-crank and four-bar mechanisms [6]

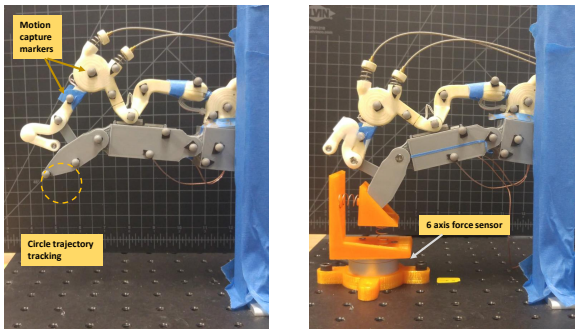

Fig. 10: Experiment setup for the trajectory tracking (left) and the fingertip force tracking experiments (right)

the measurements of finger joint angles for model validation are more accessible. Series elastic actuation is used at each actuated joint of the exoskeleton, enabling torque control using remotely located motors (RE-max 29, 22 W, Maxon Precision Motors Inc.). To perform Cartesian trajectory and force tracking at the fingertip, we only used the two actuated joints, MCP and PIP, and limited the MCP ab-ad DOF through testbed finger design.

2) Instrumented Finger: To isolate the effects of uncertainties such as relative movement at the attachments, difficulty in validating finger angles and contribution of human effort, we utilize a mechanical instrumented testbed finger (similar to [28]), rigidly attached to the exoskeleton and equipped with magneto-resistive sensors to measure the joint angles.

3) Force Sensing: To measure and validate the forces transmitted between the fingertip and the environment, we used a six-axis Robotous force/torque sensor (RFT40-SA01) with a custom designed attachment utilizing compression springs to transmit forces in two directions (Fig. 10).

4) Motion Capture: Position tracking is validated by OptiTrack motion capture system, where passive markers help determine position and orientation of the rigid bodies.

B. Experiment Protocols

Here we explain the protocol for each of the experiments.

1) Exoskeleton Joint Angle Tracking: Accurate control of the exoskeleton joint angles is the first step in achieving accurate results at the finger and Cartesian levels. However, the slack in Bowden cables results in inaccuracies. We examine the exoskeleton joint angle accuracy and compare results for the two cases of i) feedback control and ii) feedback control + backlash compensation. The desired exoskeleton joint angles are chosen as sinusoidal functions. In the first experiment, we implement a feedback control method assuming the transmission losses to be negligible. A proportional integral (PI) controller is used to control the exoskeleton joint angles with exoskeleton angle sensor data as feedback (Equation 11).

$$\theta_m = \frac{r_j}{r_m}(\theta_{j,d} - \theta_{j0}) + K_P\theta_{j,error} + K_I \int \theta_{j,error} dt \qquad (11)$$

where $\theta_{j,error} = (\theta_j - \theta_{j,d})$ is the error in exoskeleton angle tracking, and K_P and K_I are the proportional and integral gains chosen empirically.

In the second experiment, we implement the backlash inverse model to compensate for Bowden cable slack in the transmission system. We substitute the feedforward term with the smooth backlash inverse term (Equation 12).

$$\begin{aligned}\theta_m \quad = \quad & \theta_{j,d}/\alpha + c_r\gamma + c_l(1-\gamma) + K_P\theta_{j,error} \\ & + K_I \int \theta_{j,error} dt \end{aligned} \qquad (12)$$

2) Finger Joint Angle Tracking: Two control methods are compared for finger angle tracking. First, we used a simple feedback control method assuming linear proportional relationships between exoskeleton and finger joint angles (Equation 13). In practice, these relationships are nonlinear and described by kinematic models. However, as a comparison case for non-model based control, we tested this assumption.

$$\delta\theta_{exo,mcp} \approx \delta\theta_{f,mcp} \quad , \quad \delta\theta_{exo,pip} \approx -\delta\theta_{f,pip} \qquad (13)$$

In the second experiment, we implemented a model-based control taking into account the exoskeleton and finger interactions and the inverse backlash model for Bowden cable slack. The required exoskeleton angles are found based on inverse kinematics, and controlled by a PI controller using feedback from exoskeleton angles. Unlike the previous case, this method does not require finger joint angle data, which would be difficult to monitor during human-robot interaction.

3) Fingertip Position Tracking: First, we required the fingertip to follow a vertical line with a height of 1.5 cm and then a circle trajectory with a diameter of 1.5 cm in the plane of the finger. The movement frequency was 0.2 Hz, resulting in comparable speed to the human fingers during fine movements, measured empirically. The control is similar to model-based finger angle tracking with the addition of the finger inverse kinematics (Fig. 11). The feedback source used is the exoskeleton joint angle sensor data.

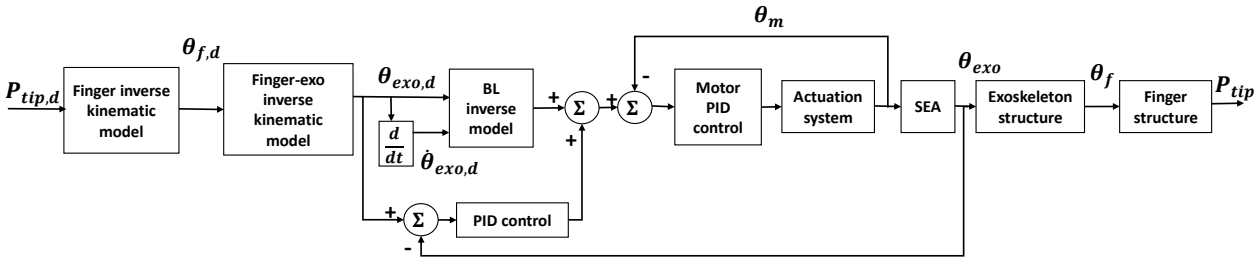

Fig. 11: Fingertip position control utilizing kinematic models and Bowden cable backlash model

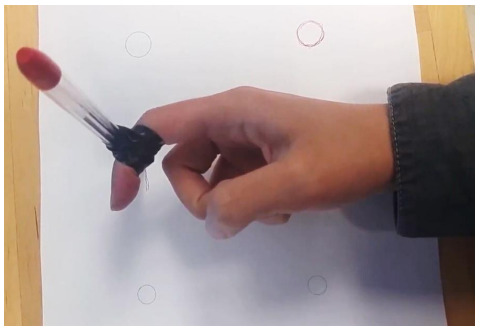

Fig. 12: Trajectory tracking task with the human finger

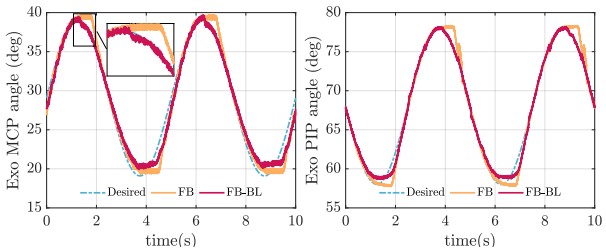

Fig. 13: Exoskeleton joint angle tracking using feedback based control (orange) vs. feedback and backlash inverse model (red)

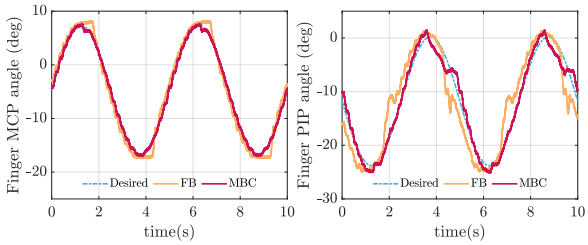

Fig. 14: Simultaneous finger angle tracking using pure feedback based control (orange) and model based control (red)

4) Human Finger Position Tracking: We had a healthy subject perform similar trajectory tracking tasks (Fig. 12). WA pen was fixed to the end of the second phalanx (similar to robot experiments). The subject traced the outlined trajectories in a periodic motion at a comfortable self-selected speed.

5) Kinematic Model Performance Evaluation: We tested the forward and inverse models by feeding them ground truth position and angle data from the motion capture system and comparing the estimated outputs with recorded motion capture values during a finger joint angle tracking task.

6) Fingertip Force Tracking: Desired fingertip forces in X and Y are determined as sinusoidal trajectories. The controller utilizes the kinematic models to calculate the configuration-dependent Jacobian of the finger and the exoskeleton. A feedback torque controller is then used to control the desired torques at the SEA.

V. Experimental Results and Discussion

First, we tested tracking performance of the motors as it sets the basis for accuracy of other controllers. The motor angle tracking percentage RMSE was calculated to be on the order of 1% and showed a slight increase with increase in speed.

Fig. 13 compares the exoskeleton angle tracking results in the feedback based control (FB) vs. simultaneous use of feedback and backlash inverse model (FB-BL). The average %RMSE values are 11.2% and 8% respectively for FB and FB-BL methods. The tracking performance is generally better for the PIP joint, since the movement of MCP joint results in moving the complete structure of the exoskeleton, whereas the PIP movement only moves the distal part of the mechanism. In the FB control of exoskeleton joint trajectories, note the errors at the peaks when the velocities change direction which are caused by slack in the transmission. Implementing the backlash inverse model noticeably improves exoskeleton angle tracking at the peaks.

Fig. 14 shows the results for simultaneous finger angle tracking. The average %RMSE values are 6.6% for the model based control (MBC) and 18.7% for the FB control. Due to the nonlinear coupling in the robot design, it is impractical to estimate the finger PIP angle based on the exoskeleton PIP angle alone, especially when MCP and PIP movements change phase, explaining the poor tracking performance in the simple FB mode. Besides the unwanted vibrations and inaccuracies in the FB mode, human finger angle measurements are not easily accessible during experiments. Alternatively, the MBC method proposed, achieves more accurate results, reducing error by 65%, and eliminates the need for finger angle measurements.

Fingertip position tracking using the MBC for vertical line

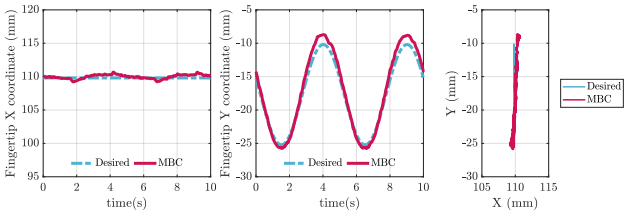

(a) Vertical line tracking

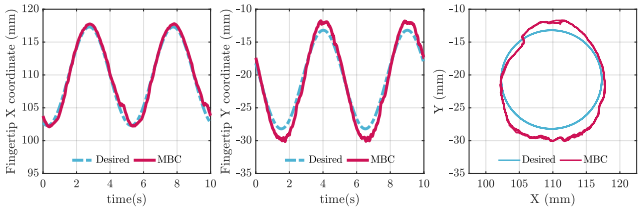

(b) Circle trajectory tracking

Fig. 15: Fingertip position tracking performance

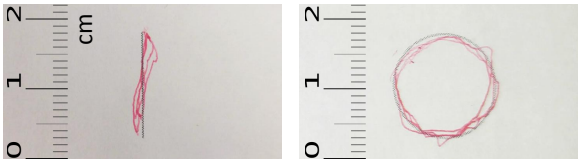

Fig. 16: Human finger performance in vertical line and circle trajectory tracking tasks

and circle trajectory are shown in Fig. 15, where average RMSE values are 0.66 mm and 0.95 mm respectively. Note that accurate fingertip position tracking was not possible without considering the nonlinear interaction models and resulted in saturation of actuators due to abrupt changes required in the control input. The remaining errors (especially in the Y direction) can be due to unmodeled weight, dynamic effects, and compliance of the transmission system. However, qualitative comparison with the tracking results of the human finger (Fig. 16) is reassuring in that the accuracies are within human finger capabilities, which are sufficient for daily tasks. Performance of the kinematic models for finger and finger-exoskeleton interaction were validated by comparing estimated values with the motion capture data. For two periods of the movement, the average %RMSE values were calculated to be 1.87% for the finger model, and 2.5% for the finger-exo interaction model. Lastly, the RMSE error for force control in X and Y directions shown in Fig. 17 is 0.142 N, illustrating that using the kinematic models of interaction and torque control at the SEA, we could control the fingertip forces in Cartesian space.

VI. Conclusion

In this research, we proposed a modeling-based approach to accurately control the fingertip position and forces through hand exoskeletons, verified the results in simulation and experimentation, and showed it's superior performance compared to the simpler feedback based control. Firstly, the

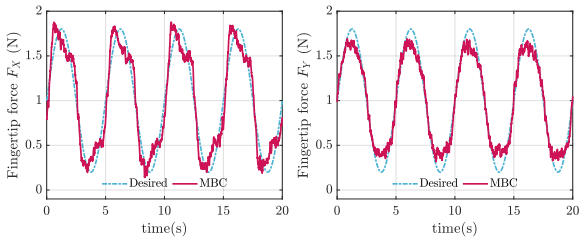

Fig. 17: Simultaneous tracking of fingertip force in X and Y directions using the model-based control

backlash inverse model for cable driven and flexible shaft actuation enables accurate control at the exoskeleton joint level. The effects of the backlash errors have also been reported in the literature [10], [9] and mentioned to greatly affect the performance of devices [8]. Secondly, implementing the kinematic and kinetic models of interaction between the finger and the exoskeleton structure allows control of the finger joint positions and torques. Thirdly, utilizing the finger models, we were able to track the fingertip position as well as direction and magnitude of the fingertip force. Unlike a few previous studies considering force control at the fingertip for haptics applications [35], [8], the method used here does not depend on force sensor feedback at the fingertip and can provide directional control of fingertip force while leaving the fingertip space open to interact with objects.

Some of our limitations and simplifying assumptions are neglecting the effects of inertia, gravity, passive and active properties of fingers, and dynamics, citing the relatively low inertia and velocities in manipulation tasks. Lack of a homing mechanism in the actuators introduced errors in determining the offsets for the backlash inverse model. For fingertip force and position control in human subject applications, a calibration phase would be required to estimate the model parameters, which are hard to measure otherwise. In future, we plan to implement similar modeling and control on human thumb and thumb exoskeleton to allow multi-finger dexterous manipulation. In addition, we will extend the model to include object space kinematics and dynamics, and stability analysis to perform in-hand manipulation.

Our work has paved the way towards improving assisted grasping and dexterous manipulation through hand exoskeletons. Using previous strategies such as finger movement coupling or limiting them to only open and close, fine control of fingertip position and forces was not possible. However, by using a model-based approach, humans would be able to fulfill dexterous manipulation tasks. Having accurate models for kinematics and kinetic relationships between the subsystems, researchers can implement various control strategies such as stiffness control or impedance control at the fingertips to improve the quality of object manipulation. Additionally, this method could be used in different realms of research such as haptics and virtual reality where the specifics of the virtual environment and the task are known.

ACKNOWLEDGMENT

This work was supported, in part, by the NSF Grant (No. NSF-CNS-1135949) and the NASA Grant (No.NNX12AM03G). The contents are solely the responsibility of the authors and do not necessarily represent the official views of the NSF or NASA.

REFERENCES

[1] M. W. Brault *et al.*, *Americans with disabilities: 2010*. US Department of Commerce, Economics and Statistics Administration, US Census Bureau Washington, DC, 2012.

[2] N. Lightdale-Miric, N. M. Mueske, S. Dayanidhi, J. Loiselle, J. Berggren, E. L. Lawrence, M. Stevanovic, F. J. Valero-Cuevas, and T. A. Wren, "Quantitative assessment of dynamic control of fingertip forces after pollicization," *Gait & posture*, vol. 41, no. 1, pp. 1–6, 2015.

[3] N. Benjuya and S. B. Kenney, "Myoelectric hand orthosis," *JPO: Journal of Prosthetics and Orthotics*, vol. 2, no. 2, pp. 149–154, 1990.

[4] M. DiCicco, L. Lucas, and Y. Matsuoka, "Comparison of control strategies for an emg controlled orthotic exoskeleton for the hand," in *Robotics and Automation, 2004. Proceedings. ICRA'04. 2004 IEEE International Conference on*, vol. 2. ieee, 2004, pp. 1622–1627.

[5] Y. Hasegawa, Y. Mikami, K. Watanabe, and Y. Sankai, "Five-fingered assistive hand with mechanical compliance of human finger," in *Robotics and Automation, 2008. ICRA 2008. IEEE International Conference on*. IEEE, 2008, pp. 718–724.

[6] Y. Yun, S. Dancausse, P. Esmatloo, A. Serrato, C. A. Merring, P. Agarwal, and A. D. Deshpande, "Maestro: An emg-driven assistive hand exoskeleton for spinal cord injury patients," in *Robotics and Automation (ICRA), 2017 IEEE International Conference on*. IEEE, 2017, pp. 2904–2910.

[7] F. Wang, C. L. Jones, M. Shastri, K. Qian, D. G. Kamper, and N. Sarkar, "Design and evaluation of an actuated exoskeleton for examining motor control in stroke thumb," *Advanced Robotics*, vol. 30, no. 3, pp. 165–177, 2016.

[8] J. Li, S. Wang, J. Wang, R. Zheng, Y. Zhang, and Z. Chen, "Development of a hand exoskeleton system for index finger rehabilitation," *Chinese journal of mechanical engineering*, vol. 25, no. 2, pp. 223–233, 2012.

[9] P. Agarwal, J. Fox, Y. Yun, M. K. O'Malley, and A. D. Deshpande, "An index finger exoskeleton with series elastic actuation for rehabilitation: Design, control and performance characterization," *The International Journal of Robotics Research*, vol. 34, no. 14, pp. 1747–1772, 2015. [Online]. Available: https://doi.org/10.1177/0278364915598388

[10] F. Wang, M. Shastri, C. L. Jones, V. Gupta, C. Osswald, X. Kang, D. G. Kamper, and N. Sarkar, "Design and control of an actuated thumb exoskeleton for hand rehabilitation following stroke," in *Robotics and Automation (ICRA), 2011 IEEE International Conference on*. IEEE, 2011, pp. 3688–3693.

[11] C. L. Jones, F. Wang, R. Morrison, N. Sarkar, and D. G. Kamper, "Design and development of the cable actuated finger exoskeleton for hand rehabilitation following stroke," *IEEE/ASME Transactions on Mechatronics*, vol. 19, no. 1, pp. 131–140, 2014.

[12] P. Polygerinos, Z. Wang, K. C. Galloway, R. J. Wood, and C. J. Walsh, "Soft robotic glove for combined assistance and at-home rehabilitation," *Robotics and Autonomous Systems*, vol. 73, pp. 135–143, 2015.

[13] M. Gabardi, M. Solazzi, D. Leonardis, and A. Frisoli, "Design and evaluation of a novel 5 dof underactuated thumb-exoskeleton," *IEEE Robotics and Automation Letters*, vol. 3, no. 3, pp. 2322–2329, 2018.

[14] L. Lucas, M. DiCicco, and Y. Matsuoka, "An EMG-controlled hand exoskeleton for natural pinching," *Journal of Robotics and Mechatronics*, vol. 16, pp. 482–488, 2004.

[15] R. Conti, E. Meli, and A. Ridolfi, "A novel kinematic architecture for portable hand exoskeletons," *Mechatronics*, vol. 35, pp. 192–207, 2016.

[16] R. Zheng and J. Li, "Kinematics and workspace analysis of an exoskeleton for thumb and index finger rehabilitation," in *Robotics and Biomimetics (ROBIO), 2010 IEEE International Conference on*. IEEE, 2010, pp. 80–84.

[17] N. Miyata, M. Kouchi, T. Kurihara, and M. Mochimaru, "Modeling of human hand link structure from optical motion capture data," in *2004 IEEE/RSJ International Conference on Intelligent Robots and Systems (IROS)(IEEE Cat. No. 04CH37566)*, vol. 3. IEEE, 2004, pp. 2129–2135.

[18] S. Cobos, M. Ferre, M. S. Uran, J. Ortego, and C. Pena, "Efficient human hand kinematics for manipulation tasks," in *Intelligent Robots and Systems, 2008. IROS 2008. IEEE/RSJ International Conference on*. IEEE, 2008, pp. 2246–2251.

[19] J. Lin, Y. Wu, and T. S. Huang, "Modeling the constraints of human hand motion," in *Human Motion, 2000. Proceedings. Workshop on*. IEEE, 2000, pp. 121–126.

[20] F. Chen Chen, S. Appendino, A. Battezzato, A. Favetto, M. Mousavi, and F. Pescarmona, "Constraint study for a hand exoskeleton: human hand kinematics and dynamics," *Journal of Robotics*, vol. 2013, 2013.

[21] T. D. Niehues, "Achieving human-like dexterity in robotic hands: inspiration from human hand biomechanics and neuromuscular control," Ph.D. dissertation, ME Dept. , UT Austin, Texas, 2017.

[22] Y. Yun, P. Agarwal, and A. D. Deshpande, "Accurate, robust, and real-time pose estimation of finger," *Journal of Dynamic Systems, Measurement, and Control*, vol. 137, no. 3-35, p. 034505, 2015.

[23] S.-W. Pu, S.-Y. Tsai, and J.-Y. Chang, "Design and development of the wearable hand exoskeleton system for rehabilitation of hand impaired patients," in *Automation Science and Engineering (CASE), 2014 IEEE International Conference on*. IEEE, 2014, pp. 996–1001.

[24] M. Cempini, M. Cortese, and N. Vitiello, "A powered finger–thumb wearable hand exoskeleton with self-aligning joint axes," *IEEE/ASME Transactions on mechatronics*, vol. 20, no. 2, pp. 705–716, 2015.

[25] M. Cempini, A. Marzegan, M. Rabuffetti, M. Cortese, N. Vitiello, and M. Ferrarin, "Analysis of relative displacement between the hx wearable robotic exoskeleton and the user's hand," *Journal of neuroengineering and rehabilitation*, vol. 11, no. 1, p. 147, 2014.

[26] J. Li, R. Zheng, Y. Zhang, and J. Yao, "iHandRehab: An interactive hand exoskeleton for active and passive rehabilitation," in *2011 IEEE International Conference on Rehabilitation Robotics*, June 2011, pp. 1–6.

[27] A. Wege and G. Hommel, "Development and control of a hand exoskeleton for rehabilitation of hand injuries," in *2005 IEEE/RSJ International Conference on Intelligent Robots and Systems*. IEEE, 2005, pp. 3046–3051.

[28] Y. Yun, P. Agarwal, J. Fox, K. E. Madden, and A. D. Deshpande, "Accurate torque control of finger joints with ut hand exoskeleton through bowden cable sea," in *Intelligent Robots and Systems (IROS), 2016 IEEE/RSJ International Conference on*. IEEE, 2016, pp. 390–397.

[29] P. Esmatloo, "Fingertip position and force control for dexterous manipulation through accurate modeling of hand-exoskeleton-environment," Master's thesis, ME Dept. , UT Austin, Texas, 2019.

[30] A. D. Deshpande, Z. Xu, M. J. v. Weghe, B. H. Brown, J. Ko, L. Y. Chang, D. D. Wilkinson, S. M. Bidic, and Y. Matsuoka, "Mechanisms of the anatomically correct testbed hand," *IEEE/ASME Transactions on Mechatronics*, vol. 18, no. 1, pp. 238–250, 2013.

[31] J. J. Craig, "Introduction to robotics: Manipulation and control," 1986.

[32] P. Agarwal, Y. Yun, J. Fox, K. Madden, and A. D. Deshpande, "Design, control, and testing of a thumb exoskeleton with series elastic actuation," *The International Journal of Robotics Research*, vol. 36, no. 3, pp. 355–375, 2017.

[33] R. L. Norton and S. S.-L. Wang, *Design of machinery: an introduction to the synthesis and analysis of mechanisms and machines*. McGraw-Hill Higher Education, 2004.

[34] P. Agarwal, Y. Yun, J. Fox, K. Madden, and A. D. Deshpande, "Design, control, and testing of a thumb exoskeleton with series elastic actuation," *The International Journal of Robotics Research*, vol. 36, no. 3, pp. 355–375, 2017. [Online]. Available: https://doi.org/10.1177/0278364917694428

[35] M. Fontana, S. Fabio, S. Marcheschi, and M. Bergamasco, "Haptic hand exoskeleton for precision grasp simulation," *Journal of Mechanisms and Robotics*, vol. 5, no. 4, p. 041014, 2013.